nature materials

SUPPLEMENTARY INFORMATION

DOI: 10.1038/NMAT2742

Free floating ultra-thin two-dimensional crystals from sequence-specific peptoid polymers

Ki Tae Nam[1], Sarah A. Shelby[1], Philip H. Choi[1], Amanda B. Marciel[1], Ritchie Chen[1], Li Tan[1], Tammy K. Chu[1], Ryan A. Mesch[1], Byoung-Chul Lee[1], Michael D. Connolly[1], Christian Kisielowski[2], Ronald N. Zuckermann[1]*

Molecular Foundry[1] and National Center for Electron Microscopy[2],
Lawrence Berkeley National Laboratory, Berkeley, California 94720, USA

* Correspondence and requests for materials should be addressed to R.N.Z. (e-mail: rnzuckermann@lbl.gov)

DOI: 10.1038/NMAT2742

CONTENTS

DOI: 10.1038/NMAT2742

A. MATERIALS

A1. Peptoid Synthesis

Peptoid oligomers were synthesized on an automated robotic synthesizer using the solid-phase submonomer method [*Ref.* R. N. Zuckermann, J. M. Kerr, S. B. H. Kent, W. H. Moos, *J. Am. Chem. Soc.* **114**, 10646 (1992)]. In this method, the Fmoc group on Rink amide resin (0.57 mmol/g, Novabiochem, San Diego, CA) was deprotected with 20% 4-methylpiperidine in DMF before starting the submonomer cycle. Peptoid synthesis on resin was carried out as follows: a 0.6 M solution of bromoacetic acid in DMF (1.13 mL in DMF, 1.35 mmol) and 0.93 eq. of N, N'-diisopropylcarbodiimide (DIC) (0.20 mL, 1.25 mmol) was added to a resin-bound amine (50 μmol) and mixed for 20 min at 35˚C during the acylation step of the submonomer cycle. The resin-bound bromide was then displaced with the amine submonomer by adding a 1.5 M solution of the amine (0.85 mL) in N-methylpyrrolidinone (NMP). This displacement reaction was carried out for 90 minutes at 35˚C. The crude peptoid products were cleaved from the resin with 95:5 trifluoroacetic acid (TFA)/water (v/v) for twenty minutes to three hours at room temperature depending on the number of t-butyl esters. The cleavage solution was filtered and evaporated under a stream of nitrogen gas to remove the TFA. The crude peptoid product was then dissolved in a 1:1 mixture (v/v) of water and acetonitrile and subjected to further purification through reverse-phase HPLC on a Vydac C4 column (10 μm, 22 mm × 250 mm), using a gradient of 10-65% acetonitrile in H_2O with 0.5% TFA over 40 min. All final products were analyzed by analytical reverse-phase HPLC (5–95% gradient at 1 mL/min over 50 minutes at 60˚C with a C4, 5 μm, 50 × 2 mm column) and matrix-assisted laser desorption/ionization mass spectrometry (Applied Biosytem/MDS SCIEX 4800 MALDI TOF/TOF Analyzer). The final peptoid products were lyophilized, dissolved in a suitable solvent and stored at –20˚C.

B. METHODS

B1. Mixing Schemes for Sheet Formation

Initial experiments examined the variations by which $(Nae\text{-}Npe)_{18}$ and $(Nae\text{-}Npe)_{18}$ could be mixed together in order to produce maximum sheet yield and quality. External parameters such as order of addition and type of container were varied. It was determined that none of these external conditions had an observable effect on sheet yield or quality. The peptoid molecules self-assembled in glass, plastic, or metal reaction chambers, with slow addition or direct pipetting into solution, and in any order of mixing. Through these initial experiments, the most simplistic external mixing scheme was chosen: fast pipetman addition in a 4 mL glass vial, followed by gentle agitatioin.

Solution conditions for sheet assembly were tested by varying pH, ionic strength, and concentration. The ratio of peptoid concentration appears integral for sheet yield. It was observed that even a 10% mismatch of the relative concentrations of $(Nae\text{-}Npe)_{18}$ and $(Nce\text{-}Npe)_{18}$ can decrease sheet population significantly. The concentrations of the peptoid stock solutions were determined by absorbance at 260 nm. The molar extinction coefficients (ε) of $(Nae\text{-}Npe)_{18}$ and $(Nce\text{-}Npe)_{18}$ at 260 nm are 310 $M^{-1}cm^{-1}$ and 293 $M^{-1}cm^{-1}$ respectively in Tris-HCl buffer (100 mM, pH 9.0) at room temperature. Typically $(Nae\text{-}Npe)_{18}$ and $(Nce\text{-}Npe)_{18}$ solutions are mixed to a final concentration of 100 μM in each, although high sheet yield was observed up to 1 M. Varying the solution pH from 4-13 revealed high sheet yield in the range of pH 8-10, with consistently high yield at pH 9. In order to obtain the highest sheet yield and quality the optimal assembly conditions are: final concentration of 0.1 mM $(Nae\text{-}Npe)_{18}$ and $(Nce\text{-}Npe)_{18}$ in 100mM pH 9 Tris buffer.

DOI: 10.1038/NMAT2742

An important step to achieve high yield and reproducibility of sheet formation was the replacement of trifluoroacetate counterions of $(Nae\text{-}Npe)_{18}$, with chloride. HPLC-purified $(Nae\text{-}Npe)_{18}$ is in the trifluoroacetate salt form. To exchange to chloride, the peptoid was dissolved in a solution of 100 mM HCl and lyophilized. The HCl treatment was repeated two times to ensure the complete replacement of trifluoroacetate counterions with chloride.

B2. Sheet Stability

The sheets showed physical stability against a variety of conditions as monitored by fluorescence microscopy. Sheets maintained a planar structure against 30 min sonication at 105W and at up to 50% acetonitrile in water. The effects of stability in methanol did not present as sharp a transition as with acetonitrile. XRD analysis showed that the sheets were still crystalline in up to 50% methanol/water mixture, but even in 60% to 80% methanol the sheets aggregated but did not completely dissolve. Sheets evaporated and dried on a Si wafer were observed to melt at 215 ºC when exposed to the air.

B3. Sheet Formation Conditions

To study the role of the electrostatic interactions in sheet formation, the ionic strength was varied. Sheets formation was observed above 500 mM NaCl and even up to 1M. They maintained the same or larger average surface area as sheets formed with low salt, but the population of sheets was significantly lessened with increased ionic strength. At 4 ºC, the rate of nucleation was high relative to the lateral growth of the sheet, resulting in many small sheets. Between room temperature and 50 ºC, the growth rate increased, resulting in fewer, larger sheets. Above 50 ºC, peptoids no longer formed sheets and instead remained as aggregates.

B4. Atomic Force Microscope (AFM) and Scanning Electron Microscope (SEM)

For Atomic force microscopy (AFM) and scanning electron microscopy (SEM) imaging, peptoid sheet containing solutions were dropped on plasma treated Si substrates. After a ten minute incubation, the substrates were gently washed with deionized water to remove salt. An Asylum MFP-3D Atomic Force Microscope was used for tapping mode imaging. A Zeiss Gemini Ultra-55 Analytical Scanning Electron Microscope was used with an in-lens detector and beam energies between 1kV and 3kV.

B5. Fluorescence Imaging

Nile Red, an environmentally-sensitive dye whose fluorescence intensity increases substantially when it is localized in hydrophobic environments, was used at a final concentration of 1 μM to stain the sheets for imaging. The solutions were dropped onto pre-cleaned microscope slides and imaged under epifluorescence illumination with an Olympus IX81 inverted microscope fitted with an Andor iXonEM+ EMCCD camera. Once loaded onto the microscope slide, sample solutions were covered with a coverslip and allowed to sit undisturbed for twenty minutes to one hour to allow the sheets to completely settle onto the surface. For a typical 0.1mM peptoid sheet preparation, the coverage of sheets on the microscope slide can be fairly high. Figure S16 shows a representative image of such a sample. For sheet surface area experiments, image thresholding and surface area measurements were performed in Adobe Photoshop.

DOI: 10.1038/NMAT2742

B6. Dye Conjugation to Peptoids

AlexaFluor 555- conjugated (Nae-Npe)$_2$-Nse-Npe-(Nae-Npe)$_{15}$

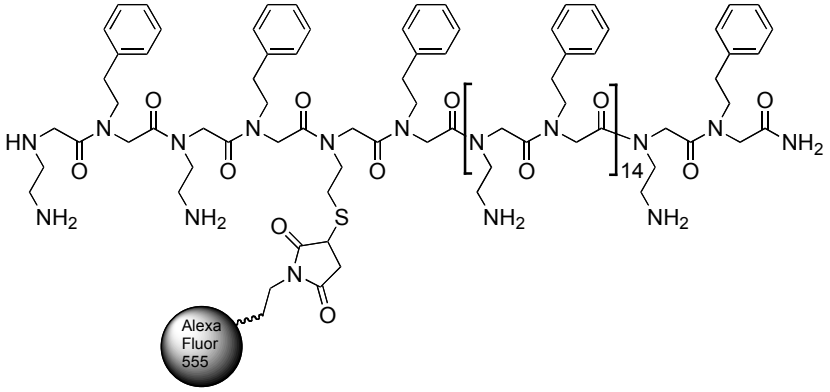

AlexaFluor 647- conjugated (Nce-Npe)$_2$-Nse-Npe-(Nce-Npe)$_{15}$

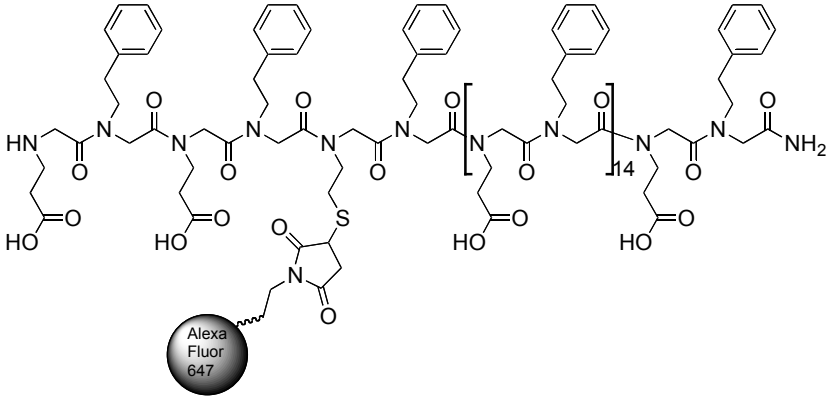

(Nae-Npe)$_2$-Nse-Npe-(Nae-Npe)$_{15}$ and (Nce-Npe)$_2$-Nse-Npe-(Nce-Npe)$_{15}$ were synthesized by substitution of the solvent-exposed 5th position of the sheet-forming 36mers with N-(2-mercaptoethyl)glycine (Nse). S-trityl-2-mercaptoethylamine was used as the submonomer at position 5 and was prepared by the method of Maltese et al. [*Ref.* M. Maltese, *J. Org. Chem.* **66**, 7615 (2001)]. AlexaFluor® 555 and AlexaFluor® 647 dyes (in maleimide form, Invitrogen) were conjugated with the HPLC-purified (Nae-Npe)$_2$-Nse-Npe-(Nae-Npe)$_{15}$ and (Nce-Npe)$_2$-Nse-Npe-(Nce-Npe)$_{15}$ peptoids, respectively [*Ref.* D. G. Smyth *et al.,*

Biochem. J. **91**, 589, (1964)]. Both reactions were purified to more than 95% homogeneity by reversed-phase HPLC as previously described.

B7. Förster Resonance Energy Transfer (FRET) Experiment

To study the kinetics of peptoid rearrangement during sheet formation, a Förster Resonance Energy Transfer(FRET) experiment was performed using AlexaFluor® 555-conjugated $(Nae\text{-}Npe)_2$-Nse-Npe-$(Nae\text{-}Npe)_{15}$ as the donor molecule and AlexaFluor® 647-conjugated $(Nce\text{-}Npe)_2$-Nse-Npe-$(Nce\text{-}Npe)_{15}$ as the acceptor. A sample was prepared consisting of 0.1 mM $(Nae\text{-}Npe)_{18}$ and $(Nce\text{-}Npe)_{18}$ containing a small fraction of each dye-conjugated peptoid. 0.2 mM solutions of $(Nae\text{-}Npe)_{18}$ and $(Nce\text{-}Npe)_{18}$ were made containing 0.1% and 0.4% AlexaFluor® 555 and AlexaFluor® 647-conjugated peptoids, respectively. The fluorescence emission spectrum, excited at 530nm, was measured minutes after these solutions were mixed and at one hour intervals from the time of mixing. A control sample lacking the acceptor dye-conjugated peptoid was run in parallel.

FRET efficiency was calculated using the ratio of donor fluorescence in the presence and absence of the acceptor molecule according to the following equation:

$$E = 1 - \frac{F'_d}{F_d}$$

Where E is the FRET efficiency, F'_d is the donor fluorescence with the acceptor dye present, and F_d is the donor fluorescence in the absence of the acceptor.

Because FRET is a distance-dependent phenomenon, changes in FRET efficiency over time indicate a change in the average distance between the donor and acceptor fluorophores and hence some change in intermolecular spacing or arrangement. As the peptoid complexes transform from small (hundreds of

DOI: 10.1038/NMAT2742

nanometers in diameter) three-dimensional aggregates to sheet structures which are spread out in two dimensions at bilayer thickness, the average spacing between donor and acceptor dyes, which are sparsely populated in the sheet structure compared to the bulk peptoid, should drastically increase. As a result, the FRET efficiency should decrease over time. By twelve hours after mixing, the FRET efficiency has significantly decreased, indicating that the sample mostly consists of sheets. The time scale of this behavior as observed by FRET measurements is consistent with the time scale of sheet formation as observed by fluorescence microscopy.

When both AlexaFluor 555 and 647-labeled peptoids are incorporated into the sheets, the fact that fluorescence of both dyes is observed in an individual sheet further indicates that sheets are composed of both complementary sequences: $(Nae\text{-}Npe)_{18}$ and $(Nce\text{-}Npe)_{18}$.

B8. XRD Analysis

(a) Powder XRD

X-ray diffraction data were collected at a multiple-wavelength anomalous diffraction and monochromatic macromolecular crystallography beamline, 8.3.1, at the Advanced Light Source located at Lawrence Berkeley National Laboratory. Beamline 8.3.1 has a 5 tesla single pole superbend source with an energy range of 2.4-18 keV. Data were collected with a 3 x 3 CCD array (ADSC Q315r) detector at a wavelength of 1.1159 Å. Data sets were collected at 200-mm distances with 40s exposure times and 1 degree oscillations on a bulk sample of peptoid sheet. Peptoid sheet containing solutions were centrifuged at 13,200 rpm for 10 minutes. The resulting peptoid sheet pellet was then collected on a 0.2-0.3 mm diameter nylon loop. Data was processed in Igor Pro 6.0 with a silver behenate (AgBE) standard.

(b) Solution XRD

The solution X-ray scattering experiments were performed using the 7.3.3 beamline at the Advanced Light Source at Lawrence Berkeley National Laboratory. To prevent the aggregation or stacking at high concentration, the sheet were produced initially using 10 μM concentrations of $(Nce\text{-}Npe)_{18}$ and $(Nae\text{-}Npe)_{18}$ in 10 mM AMPD buffer (100 mM NaCl and pH9.0) and concentrated using Amicon centrifuge filter (Millipore, MA, United States). Final concentration of peptoid sheet solution was 5 mg/ml as determined by the absorbance at 214 nm. The sample solution (20 μL) was loaded into a liquid cell that is made of lexan and has mica windows. The liquid cell (Peter Boyd Technologies, United States) used here was 2 mm in thickness. The scattering from the buffer solution without peptoids was measured as background and was subtracted from scattering spectra of the sheet solution. An X-ray beam of wavelength 1.24 Å (10 keV) was passed through the sample and the resulting spectra were collected with a Dectris Ltd. Pilatus 1K detector (487x195 pixels). The sample to detector distance was 198 mm. Images were radially integrated using the Nika software package in Igor Pro. To create the scattering curves, fifty images taken with 2-s exposures were averaged and normalized by the summed output of a photodiode put in front of the detector to act as a beamstop. The shadow of this photodiode was masked out during the radial integration. Radiation damage to the sample was checked by comparing the first 3 exposures to the last 3 exposures. There was no change in the scattering curve, suggesting that there was little or no radiation damage during the X-ray exposure.

DOI: 10.1038/NMAT2742

B9. TEM Analysis

We deposited the peptoid sheets on commercially available holey carbon-coated TEM grids (SPI Supplies Inc., PA). A droplet of sheet containing solution was placed on a TEM grid and incubated for 10 minutes. The excess liquid was then wicked away with filter paper. As a result, some sheets were suspended over the holes in the substrate (see Fig. S13A) and data were taken from those portions. The prepared TEM grids were kept in desiccators before TEM imagine to ensure moisture removal. We collected our data from a single layer of sheet.

Traditional microscopy (JEOL 2100F) at the Molecular Foundry and the One-Angstrom microscope (modified Philips CM300FEG) at the National Center for Electron Microscopy (NCEM) was not capable of resolving the crystalline structure of sheets. Figure S13B is the image taken from the area around the edge of the sheets using the One-Angstrom microscope. We were able to observe some degree of local ordering in a few areas but could not reveal the long range ordering of the peptoid chains in detail. There was no indication of contamination or degradation of the sample. After two exposures at the same spot, the same image was produced, suggesting stability of our sample.

The TEAM 0.5 microscope provided exceptional resolution and allowed for the detailed examination of the peptoid chains. We found that using a monochromator is critical for visualization of the peptoid chains. The exposure time was 1s. We did not observe any conformational change of the ordered peptoid chains over a period of 60 seconds.

B10. Zeta Potential Measurement

Surface charge of sheets in aqueous solution was measured. Zeta potential data was collected with a Malvern Zetasizer, model Nano ZS (Malvern Instruments Ltd., UK) with a He-Ne (633 nM) 4.0 mW laser. Data was collected with an Avalanche photodiode with Q.E. > 50% at 633 nM using the M3-PALS

measurement technique. Figure S15 show Zeta potential-pH dependence of peptoid sheets. A single 0.1mM peptoid sheet containing solution was pH adjusted by adding 1μL increments of 100mM NaOH/HCl. The solution was then transferred to a polycarbonate folded capillary cell where zeta potential measurements were taken in triplicate from pH 4.3 to 10.8.

B11. Streptavidin binding to HPQ-functionalized sheets

The *cyclo*-[CHPQFC]-modified $(Nae\text{-}Npe)_{18}$ peptoid was synthesized by automated solid-phase synthesis and purified by HPLC as described for the other polypeptoids. Disulfide formation to generate the cyclic hexapeptide was accomplished by treatement with 1 mM $K_3[Fe(CN)_6]$. The mass of 4583.5 was confirmed by electrospray LC/MS. Binding experiments were done by adding 0.4 μg of Cy3-streptavidin (Invitrogen) to 100 μL of 10 μM sheets in 100 mM Tris pH 8, and incubating for <30 min. Washing of sheets (3 x100mM Tris pH 8) was accomplished by spin filtration using Pall Corporation NanoSep 100K spin filters in an Eppendorf 5415D centrifuge. Fluorescence measurements were taken using a Horiba JobinYvon Fluoromax-4 Spectrofluorometer, with an excitation wavelength of 520 nm, and the integration of the emission curve from 530 nm to 600 nm was taken to determine Cy3 concentrations. Fluorescence images were taken using a Cy3 filter on an Olympus IX81 inverted microscope fitted with an Andor iXonEM+ EMCCD camera.

DOI: 10.1038/NMAT2742

C. PEPTOID SEQUENCES

Table S1 | Structures of the synthesized peptoids and the molecular weight of each peptoid as determined by mass spectrometry are shown below. The following monomer abbreviations were used to name the sequences:

Npe : N-(2-phenethyl)glycine

Nae: N-(2-aminoethyl)glycine

Nce: N-(2-carboxyethyl)glycine

Nme: N-(2-methoxyethyl)glycine

Nbn: N-benzylglycine

Nse: N-(2-mercaptoethyl)glycine

(Nae-Npe)$_{18}$ Molecular weight: 4720.8 (Calculated), 4721.6 (Found)

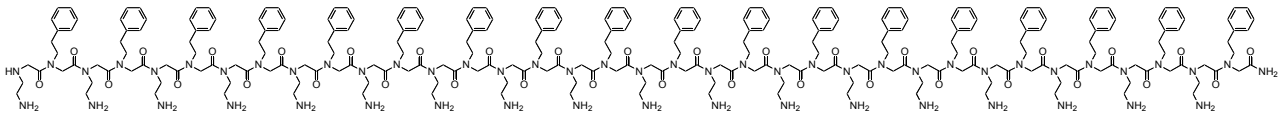

(Nce-Npe)$_{18}$ Molecular weight: 5242.7(Calculated), 5243.6 (Found)

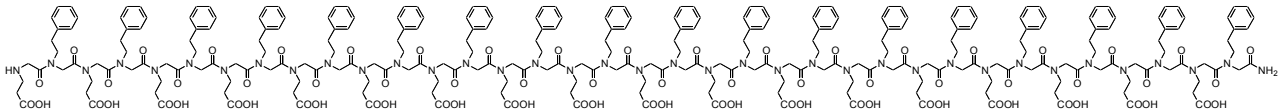

(Nae-Npe-Npe)$_{12}$ Molecular weight: 5087.3 (Calculated), 5089.2(Found)

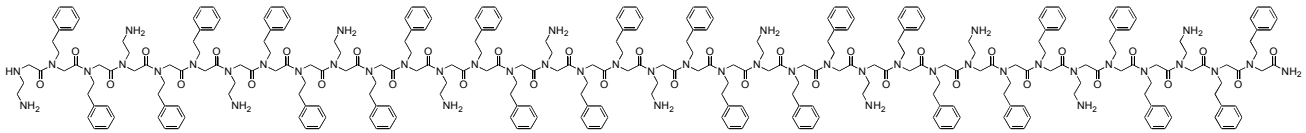

(Nce-Npe-Npe)$_{12}$ Molecular weight: 5435.2 (Calculated), 5434.5 (Found)

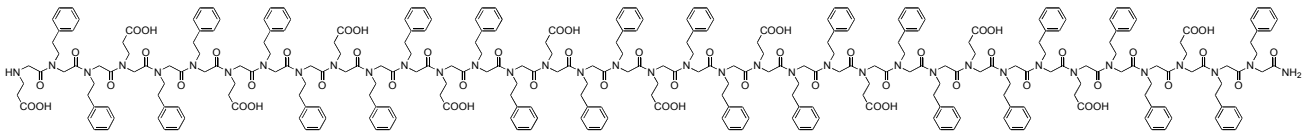

(Nae-Npe-Npe-Npe)$_9$ Molecular weight: 5270.5(Calculated), 5271.0(Found)

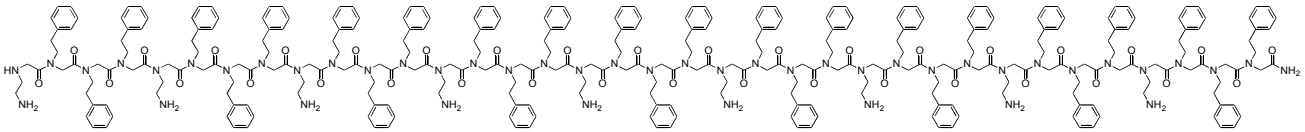

(Nce-Npe-Npe-Npe)$_9$ Molecular weight: 5531.5(Calculated), 5530.9 (Found)

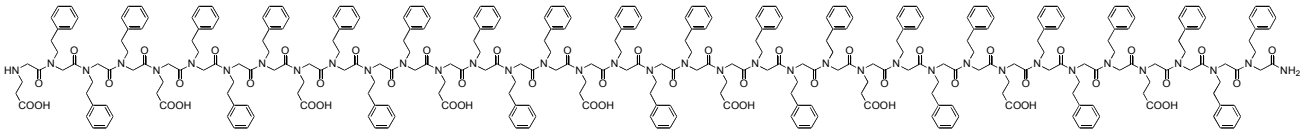

(Nce-Npe)$_9$ Molecular weight : 2629.9 (Calculated), 2631.9 (Found)

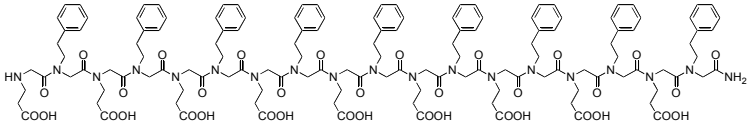

(Nae-Npe)$_9$ Molecular weight : 2368.9 (Calculated), 2370.8 (Found)

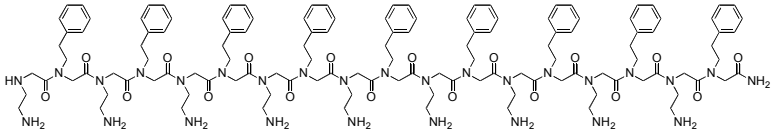

(Nce-Npe)$_6$ Molecular weight: 1758.9 (Calculated), 17662.5 (Found)

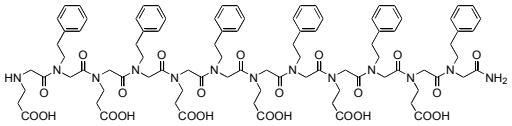

(Nae-Npe)$_6$ Molecular weight: 1584.9 (Calculated), 1588.3 (Found)

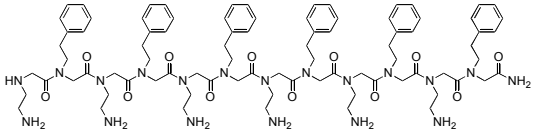

(Nce-Npe)$_3$ Molecular weight: 888.0(Calculated), 888.6 (Found)

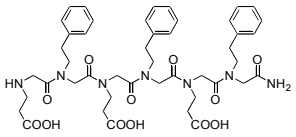

DOI: 10.1038/NMAT2742

(Nae-Npe)$_3$ Molecular weight: 801.0 (Calculated), 801.4 (Found)

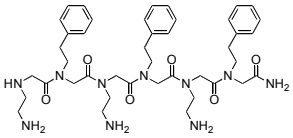

(Nae-Nme)$_{18}$ Molecular Weight: 3891.5 (Calculated), 3891.2 (Found)

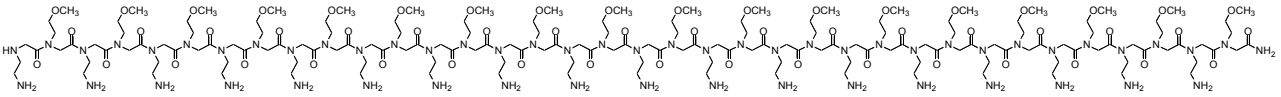

(Nce-Nme)$_{18}$ Molecular Weight: 4413.4 (Calculated), 4413.9 (Found)

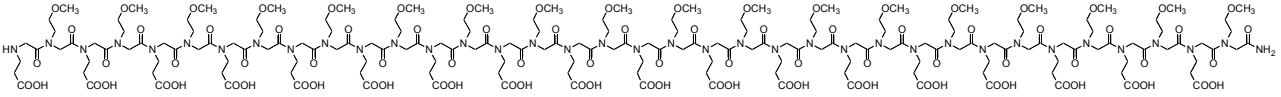

(Nme-Npe)$_{18}$ Molecular Weight: 4991.0 (Calculated), 4991.6 (Found)

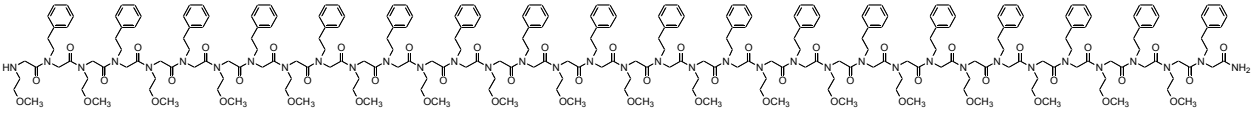

(Nce-Nbn)$_{18}$ Molecular Weight: 4990.2 (Calculated), 5002.6 (Found)

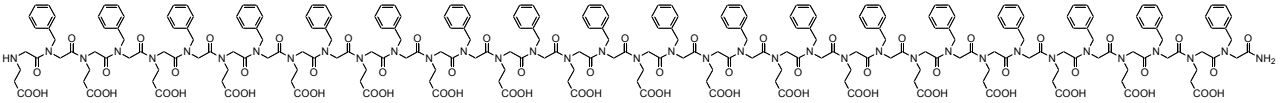

(Nae-Nbn)$_{18}$ Molecular Weight: 4468.3 (Calculated), 4469.5(Found)

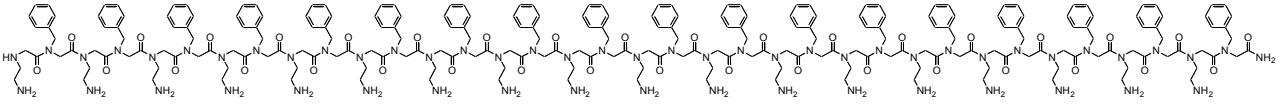

(Nce-Npe)$_2$-Nse-Npe-(Nce-Npe)$_{15}$ Molecular Weight:5230.7(Calculated), 5234.3(Found)

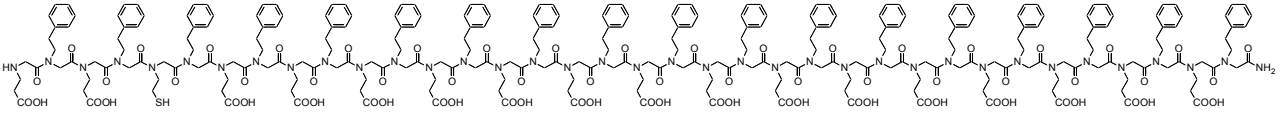

(Nae-Npe)$_2$-Nse-Npe-(Nae-Npe)$_{15}$ Molecular Weight: 4737.8 (Calculated), 4736.2 (Found)

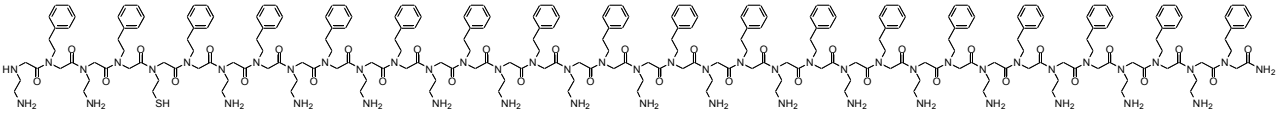

D. SUPPLEMENTARY DATA

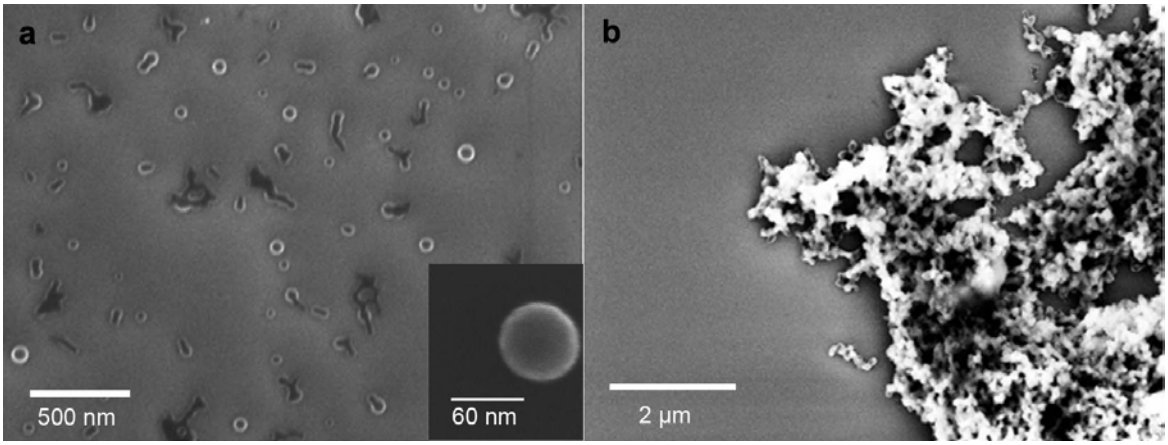

Figure S1 | SEM images of aggregates resulting from three-fold and four-fold periodic sequences. a, Mixture of $(Nae\text{-}Npe\text{-}Npe)_{12}$ and $(Nce\text{-}Npe\text{-}Npe)_{12}$ in aqueous solution. Three-fold periodicity does not produce sheets. **b,** Aggregated structures resulted by mixing $(Nae\text{-}Npe\text{-}Npe\text{-}Npe)_9$ and $(Nce\text{-}Npe\text{-}Npe\text{-}Npe)_9$. Four-fold periodicity does not generate sheets either.

DOI: 10.1038/NMAT2742

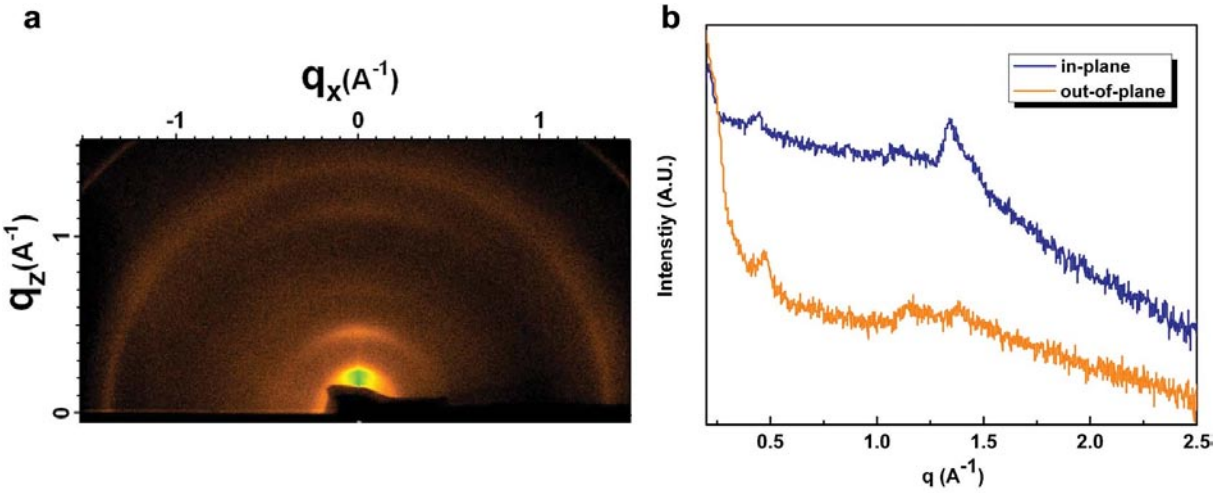

Figure S2 | Grazing Angle Incidence X-Ray Diffraction (GIXRD) data from the sheets. a, 2D image map of a GIXRD pattern. **b,** Line profiles of the scattering as a function of the scattering vector. The 2D image map of a GIXRD pattern can be divided into a component in the plane of the substrate (q_x) and a component perpendicular to the substrate (q_z). The sheet-containing solution was drop-cast on a (100) Si wafer. Drop-casting was repeated until the wafer was mostly covered by sheets. The diffraction at 0.46 $Å^{-1}$ results from the second harmonic of the sheet thickness. It shows a stronger peak in the nominally out-of-plane direction than in the in-plane direction. The peak around 1.4 $Å^{-1}$ is more intense in the in-plane direction, suggesting the ordering exists perpendicular to the sheet thickness.

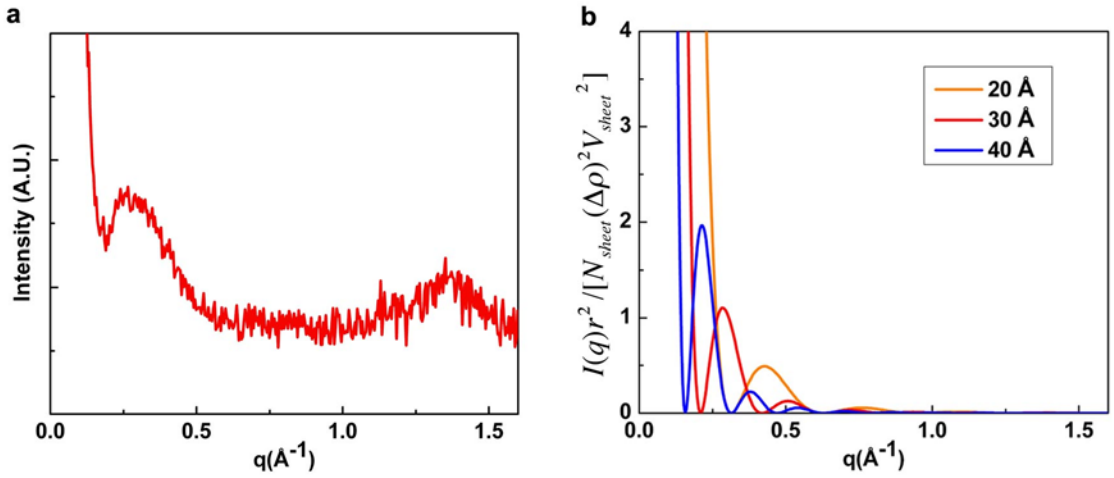

Figure S3 I X-ray scattering spectra of free-floating peptoid sheets in solution. a, Experimental data obtained from a peptoid sheet solution at a concentration of 5 mg/ml in 10 mM AMPD buffer (100 mM NaCl and pH9.0). **b**, Simulated scattering spectra based on the derived form factor of a laterally extended, thin sheet with different thicknesses of 20, 30 and 40 Å.

In Fig. S3a, the broad scattering centered at q= 0.28 $Å^{-1}$ is due to the non-Bragg scattering from individual sheets in solution. The inter-chain spacing peak is still observed at q = 1.4 $Å^{-1}$, which is the same peak position with that of powder XRD data. However, as expected, the lamellar peaks at q=0.23 $Å^{-1}$ cannot be detected.

To better understand the scattering data at low q, the previously derived form factor for a large disk was used to model the shape of spectra and the peak position (Fig. S3b). The scattering form factors of a large sheet of thickness d was employed. This model is a large disk form factor developed by Pedersen (Ref. *J. Appl. Cryst.* 33, 637-640 (2000)) and can further simplified to the following equation when the radius of disk (r) is much larger than the thickness (d) (Ref. *J. Phys. Chem. B.* **111**, 4211-4219 (2007)).

$$|F(q)|^2 = \frac{2}{(qr)^2}\left[\frac{\sin(qd/2)}{qd/2}\right]^2$$

DOI: 10.1038/NMAT2742

The scattering intensity can be described by

$$I(q) = N_{sheet}(\Delta\rho)^2 V_{sheet}{}^2 |F(q)|^2 S(q)$$

where N_{sheet} is the number density of scattering sheets, $\Delta\rho$ is the difference in scattering density between the sheets and buffer, V_{sheet} is the volume of the sheet, F(q) is the form factor from sheets, S(q) is the interparticle interference function.

In this study, the scattering intensity using the exact prefactor parameter was not determined but the first peak position was compared at the different sheet thicknesses of 20, 30, 40Å . As shown in Fig. S3b, when simulated with 30 Å thickness, the spectra provide the best fit in the first peak position. This thickness estimated from the scattering spectra is closed matched with 27 Å sheet thickness that was experimentally measured using AFM.

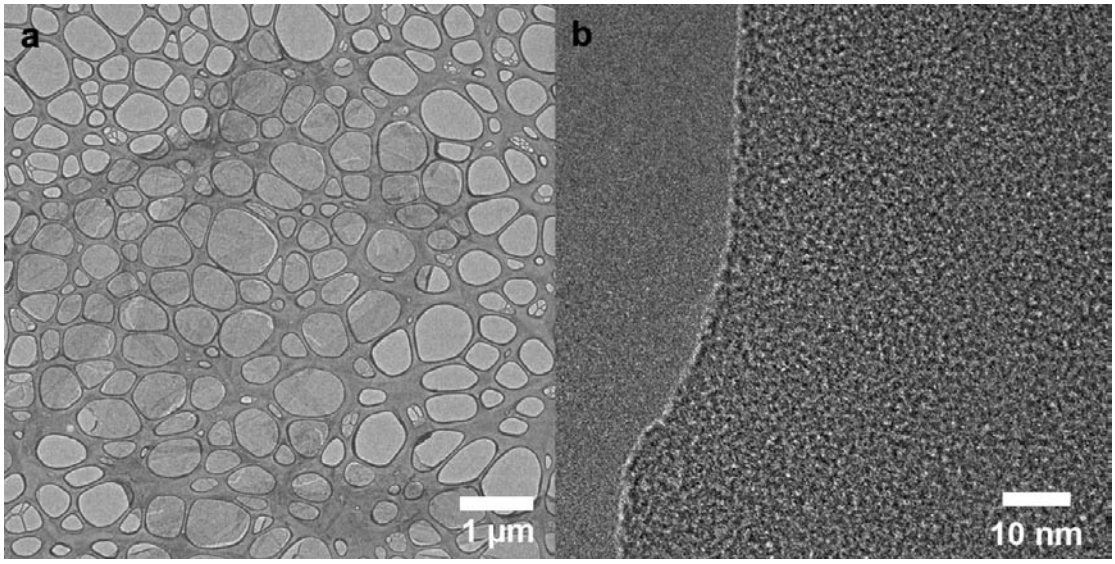

Figure S4 | **TEM analysis of a peptoid sheet. a,** TEM image of a peptoid sheet on a holey carbon-coated grid at low magnification. TEM analysis was performed on an area where a single layer of sheet was suspended over a hole. **b,** High resolution TEM image of a peptoid sheet obtained by the One-Angstrom microscope at NCEM. The image clearly shows the edge of a sheet. Local ordering was observed in some areas, but the details of peptoid chain ordering were not revealed.

DOI: 10.1038/NMAT2742

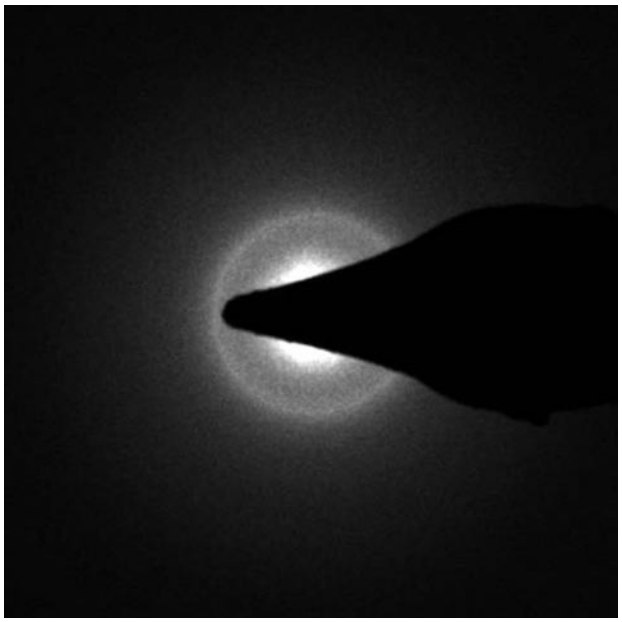

Figure S5 | **Electron Diffraction of a single sheet.** The peptoid sheets were prepared in aqueous solution as described above, and glucose was added to a final concentration of 2% (w/v). This solution was deposited on a carbon coated grid, and the excess liquid was removed by blotting with absorbent paper. To minimize electron beam damage, the Philips CM 20 transmission electron microscope was operated at 80 kV. Exposure time was 5 seconds. The major feature observed was a diffraction ring at 4.5 Å which corresponds to inter-chain distance between aligned peptoids, and matches the distances obtained by x-ray diffraction and high resolution abberation-corrected transmission electron microscopy.

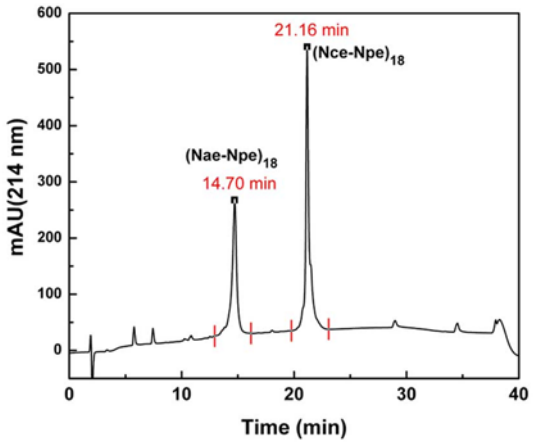

Figure S6 | Composition of $(Nae\text{-}Npe)_{18}$ and $(Nce\text{-}Npe)_{18}$ in a sheet. Analytical reverse phase HPLC chromatogram of dissociated sheets. 0.4mM of $(Nce\text{-}Npe)_{18}$ and 0.2 mM $(Nae\text{-}Npe)_{18}$ were initially mixed, yet the ratio of $(Nce\text{-}Npe)_{18}$ to $(Nae\text{-}Npe)_{18}$ in the resulting sheets is close to 1:1. Sheet composition of $(Nae\text{-}Npe)_{18}$ and $(Nce\text{-}Npe)_{18}$ in different mixing ratios: 2:1, 1:1 and 1:2 was analyzed. Regardless of the initial ratio of the two peptoids, the composition of the sheet was always close to 1:1. The ratio of $(Nae\text{-}Npe)_{18}$ to $(Nce\text{-}Npe)_{18}$ in sheet samples were determined by analytical reverse-phase HPLC at 60˚C with a C4, 5 μm, 50 × 2 mm column. The sheets were spun down from solution at 10,000 rpm for 30 min, after which the supernatant was removed. The pellet was dissolved in 50/50 acetonitrile/water (v/v) with 5mM HCl. The solution was lyophilized and the resulting powders were re-dissolved in 50/50 acetonitrile/water (v/v). Area (mAU•min) under the $(Nae\text{-}Npe)_{18}$ and $(Nce\text{-}Npe)_{18}$ peaks was integrated and the composition was calculated using the molar extinction coefficient. The molar extinction coefficients of $(Nae\text{-}Npe)_{18}$ and $(Nce\text{-}Npe)_{18}$ at 214 nm are 166 $mM^{-1}cm^{-1}$ and 237 $mM^{-1}cm^{-1}$ respectively, in 50/50 acetonitrile/water according to UV/Vis absorption spectroscopy.

DOI: 10.1038/NMAT2742

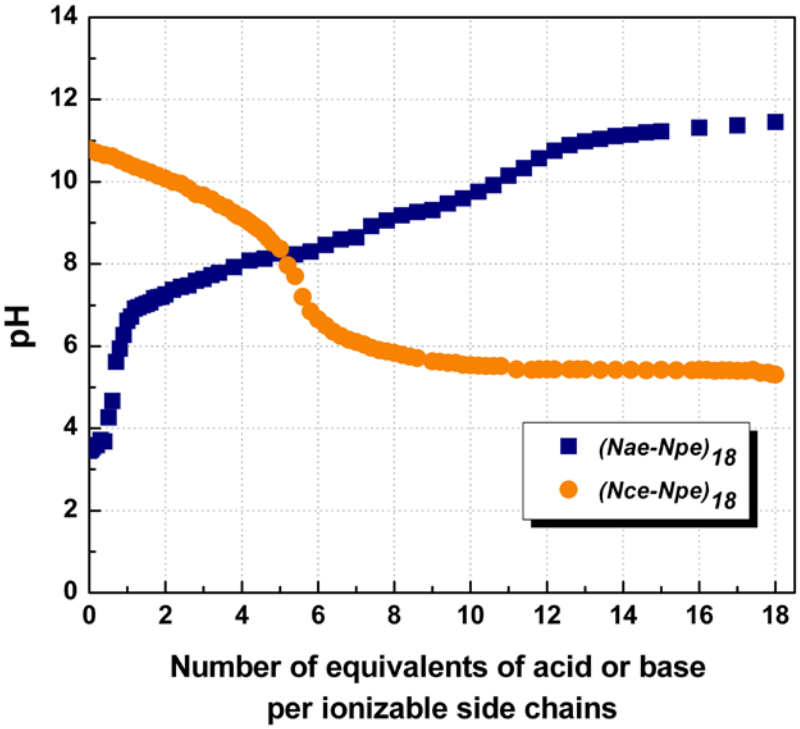

Figure S7 | Acid-base titration curve of (Nae-Npe)$_{18}$ and (Nce-Npe)$_{18}$ determined separately. The titration curve for (Nae-Npe)$_{18}$ was produced using an Accumet AB15 pH meter, starting with 1 mL of 1 mM (Nae-Npe)$_{18}$ at pH 3.5 and adding 2 μL increments of 100 mM NaOH. The titration curve for (Nce-Npe)$_{18}$ was done with the same pH meter, starting with 1 mL of 1 mM (Nce-Npe)$_{18}$ at pH 2.75 and adding 2 μL increments of 100 mM NaOH. The x-axis corresponds to the number of charged side-chains on a single peptoid based on the volume of base added. The point at pH 8.5 where the titration curves cross is where (Nae-Npe)$_{18}$ and (Nce-Npe)$_{18}$ carry equal numbers of charges. The region from pH 7 to pH 10 is where the (Nae-Npe)$_{18}$ and (Nce-Npe)$_{18}$ are similarly charged, and also corresponds to the pH region where sheet formation is optimal. At extreme pH values outside of this range, there is a large charge imbalance between the two peptoids and little sheet formation is observed.

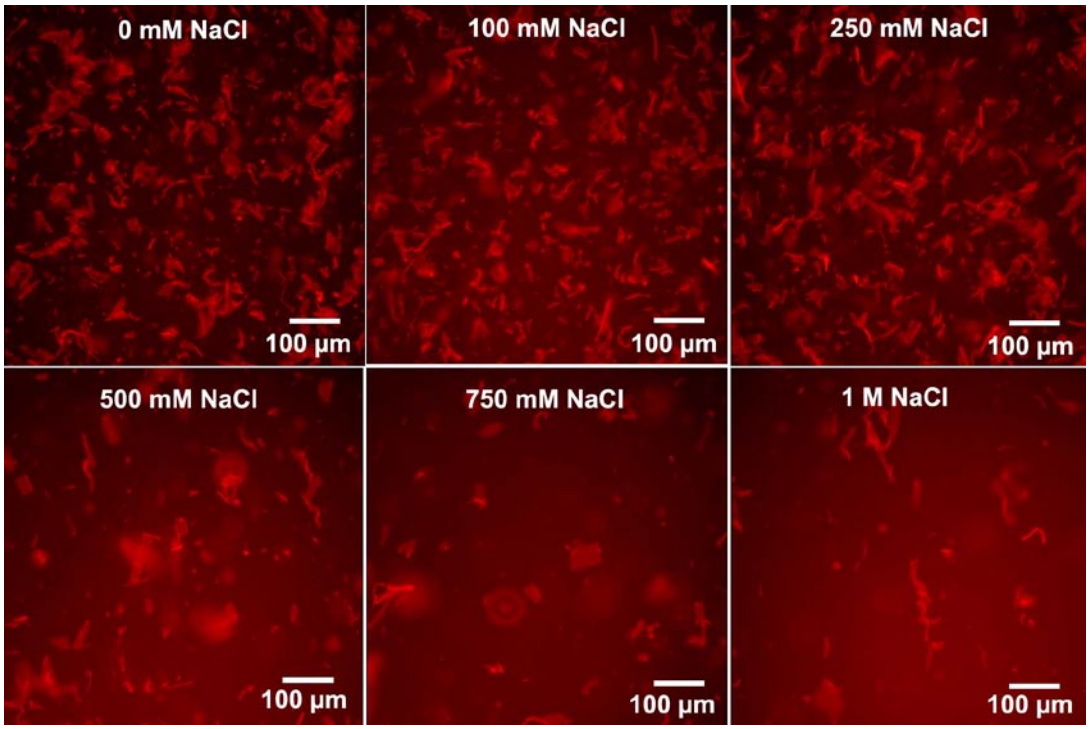

Figure S8 | Dependence of sheet formation on ionic strength studied by fluorescence optical microscopy. Ionic strength was adjusted by adding NaCl to solution. It was observed that the sheets can still form up to 1M NaCl. However, the population of sheets was lessened significantly with increased ionic strength. Additionally, the morphology of sheets became irregular aggregates above 500 mM NaCl. his dependence on ionic strength is somewhat gentle, and, taken with the broad pH dependence, suggests that the hydrophobic effects contribute significantly to sheet formation. It is likely that the effect of increased ionic strength is to lessen both the coulombic attraction between opposite charges and the repulsion between similar charges. This probably impacts the mechanism of sheet formation more than it affects the stability of the final structure. Evidence of this was noted when at high ionic strength, the initial mixing of the two oppositely charged peptoids did not result in a cloudy solution, while the mixing at the low ionic strength always generated the cloudiness. Thus, it seems likely that the size of spheres resulting from the initial complexation is significantly smaller at high ionic strength.

DOI: 10.1038/NMAT2742

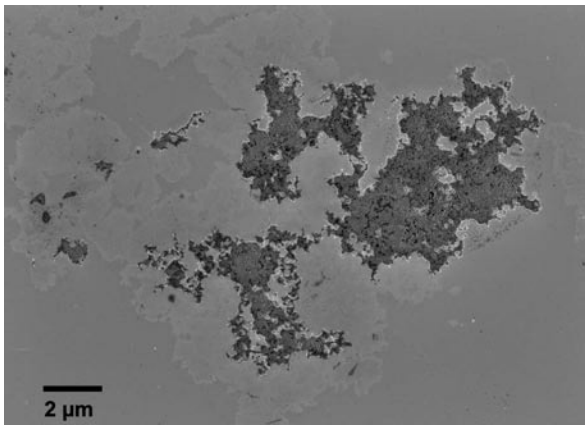

Figure S9 | SEM image of aggregates observed in the case of two fold periodic peptoid 6mers. Mixing $(Nce\text{-}Npe)_3$ and $(Nae\text{-}Npe)_3$ did not form planar structures under the typical sheet forming conditions of 36mer peptoids. The concentration of each peptoid was 0.1 mM. SEM samples were made one day after mixing. At a 5 mM peptoid concentration, some planar aggregates formed but to a much lesser degree than 36mers.

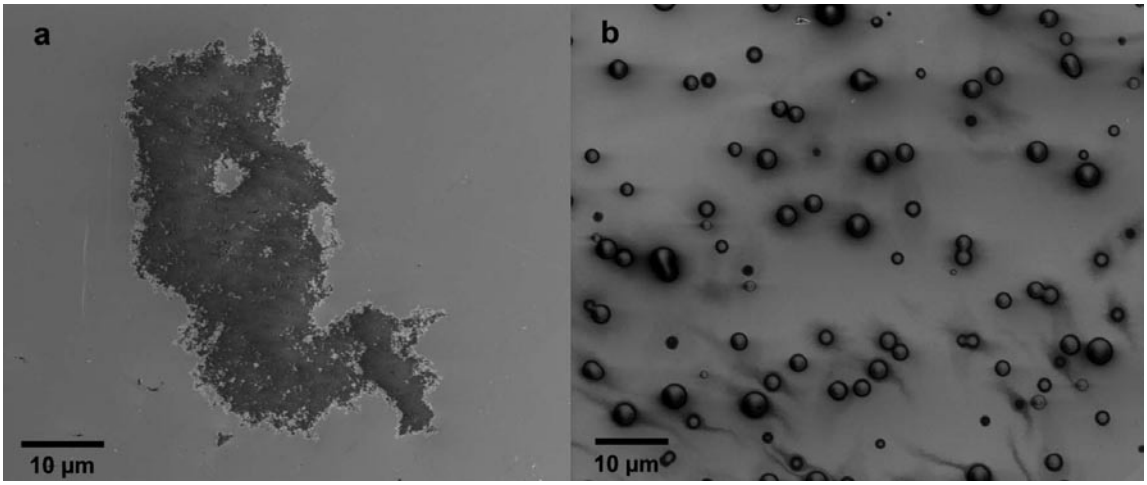

Figure S10 | Self-assembly and aggregation of control sequences. a, SEM image of the complexation of the control sequences with no hydrophobic groups, $(Nae\text{-}Nme)_{18}$ and $(Nce\text{-}Nme)_{18}$. The mixing of $(Nae\text{-}Nme)_{18}$ and $(Nce\text{-}Nme)_{18}$ in aqueous solution [Tris-HCl (pH 9.0, 100 mM)] resulted in aggregation. The concentration of each peptoid is 0.1 mM. SEM samples were made one day after mixing. **b,** SEM image of $(Nme\text{-}Npe)_{18}$ which contains no ionic groups. Because $(Nme\text{-}Npe)_{18}$ is not soluble in aqueous solution, 50 % methanol/water (v/v) was used to prepare the SEM sample.

DOI: 10.1038/NMAT2742

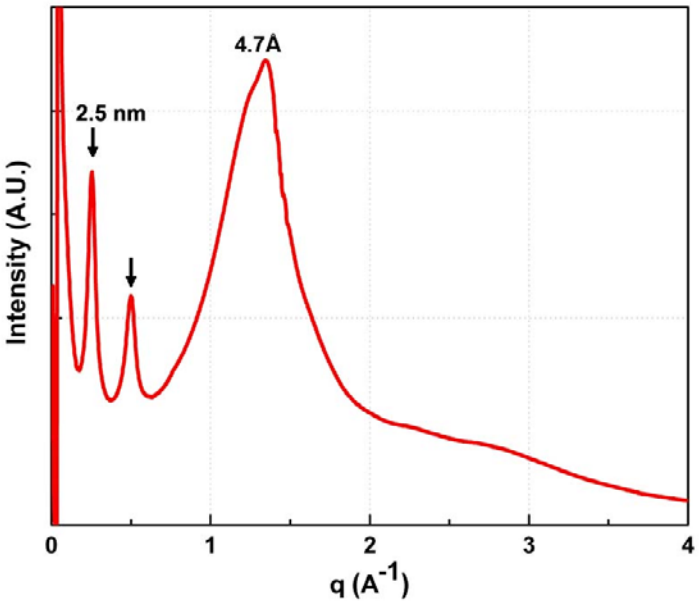

Figure S11 | XRD from sheets assembled from (Nce-Nbn)$_{18}$ and (Nae-Nbn)$_{18}$. Analogs (Nce-Nbn)$_{18}$ and (Nae-Nbn)$_{18}$ elucidated the importance of the original phenethylamine groups in the organization of the peptoid sheet hydrophobic core. X-ray diffraction revealed the thickness of the analog sheet to be 2.5 nm with a chain-chain spacing of 4.7 Å. The replacement of the phenethylamine groups with benzylamine in the analog resulted in an expected decrease in sheet thickness, corresponding to the loss of two single carbon-carbon bonds. An observed increase in chain-chain spacing can be attributed to the decrease in degrees of freedom of the benzylamine groups compared to phenethylamine. Through atomically precise peptoid synthesis we have demonstrated a tunable system that can be used to improve the crystallinity of self-assembling peptoid structures.

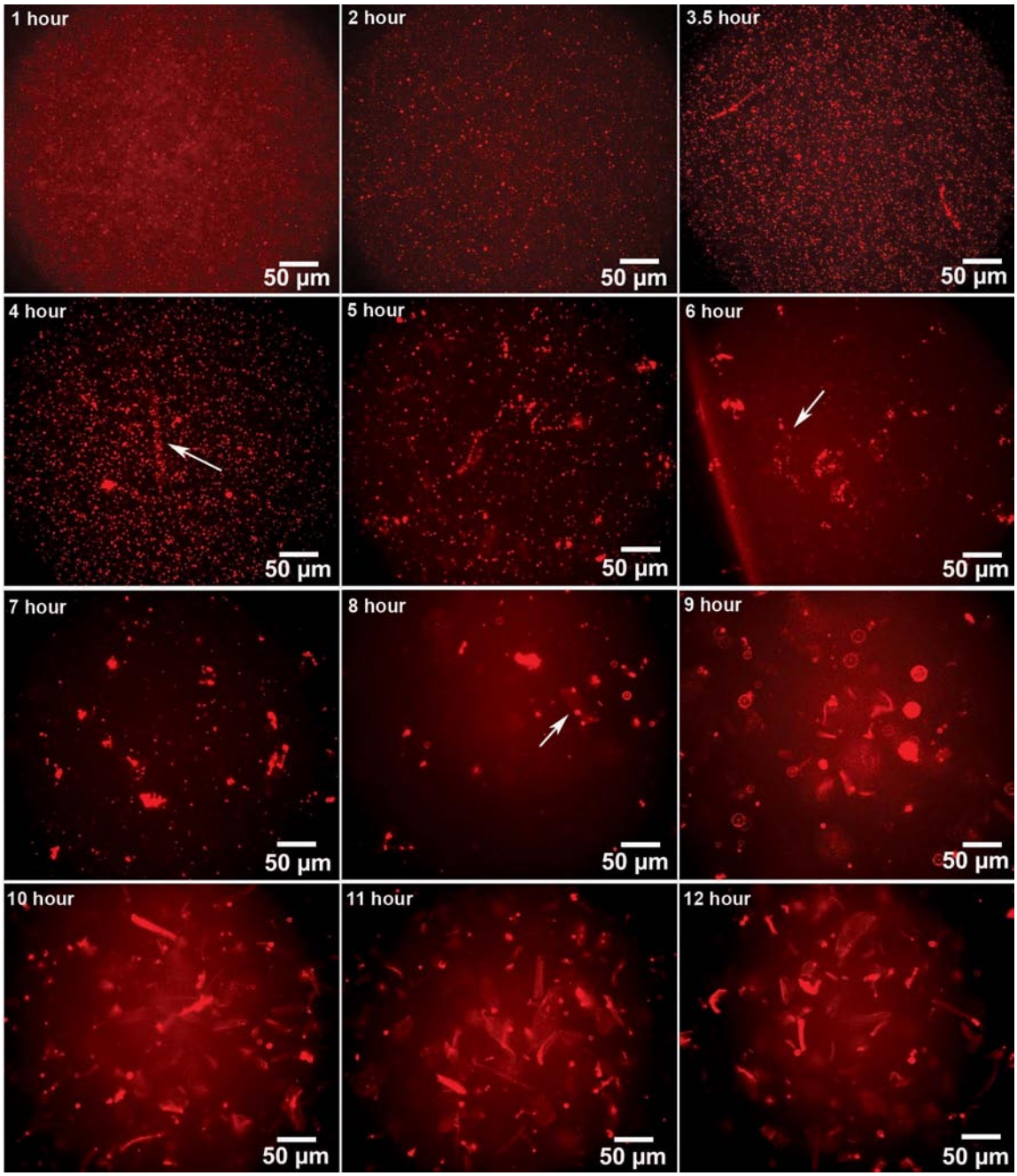

Figure S12 | A series of fluorescence microscope images acquired every hour from one to twelve hours after mixing to follow the transition from aggregates to sheets. The sample contained 0.1mM AlexaFluor® 555-conjugated (Nae-Npe)$_2$-Nse-Npe-(Nae-Npe)$_{15}$ and AlexaFluor® 647-conjugated (Nce-Npe)$_2$-Nse-Npe-(Nce-Npe)$_{15}$.Over the first 3.5 hours, the small, uniform spheres that form

DOI: 10.1038/NMAT2742

upon mixing coalesce into larger, sparser spheres which are not regularly sized. During the first three-hour lag phase, no sheet formation could be observed. Instead, an abundance of small aggregates were observed to slowly coalesce into a smaller number of larger and more distinct spherical structures. Between 3.5 and 5 hours after mixing, aggregates of aligned spheres form as indicated by the first white arrow. These aggregates become more numerous as the number of spheres decreases and begin to resemble sheets around six hours. One early sheet is pointed out by the second white arrow. The majority of material is still spherical. In the mid-growth phase after six hours, intermediate structures consisting of a sheet with multiple attached spheres begin to predominate, suggesting that large sheets are the product of more than one sphere. Typical, fully-formed sheets can be observed by eight hours after mixing. The population of sheets continues to increase between eight and twelve hours. Final sheet dimensions ranges from 10 μm to 60 μm in width and from 20 μm to 140 μm in length (Fig. 5f). Interestingly, the aspect ratio (length:width) ranges from 1:1 to 7:1, which suggest that the propagation rates along both planar dimensions are similar.

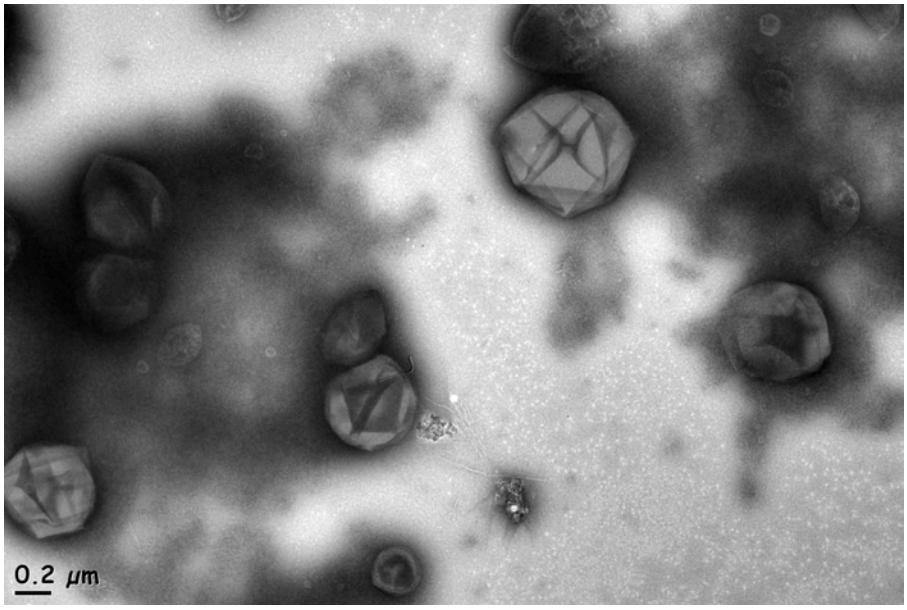

Figure S13 | TEM image of spheres found initially after mixing (Nce-Npe)$_{18}$ and (Nae-Npe)$_{18}$. Immediately after the mixing, 20 μL of the solution was dropped on a carbon coated copper grid and incubated for ten minutes to ensure the adsorption of peptoids. The grid was incubated with a droplet of negative staining solution (Nano W®, Nanoprobes Inc., Yaphank, NY) for two minutes and then with a droplet of water for two minutes. We repeated the staining procedure once and soaked up the remaining solution on the grid with filter paper.

DOI: 10.1038/NMAT2742

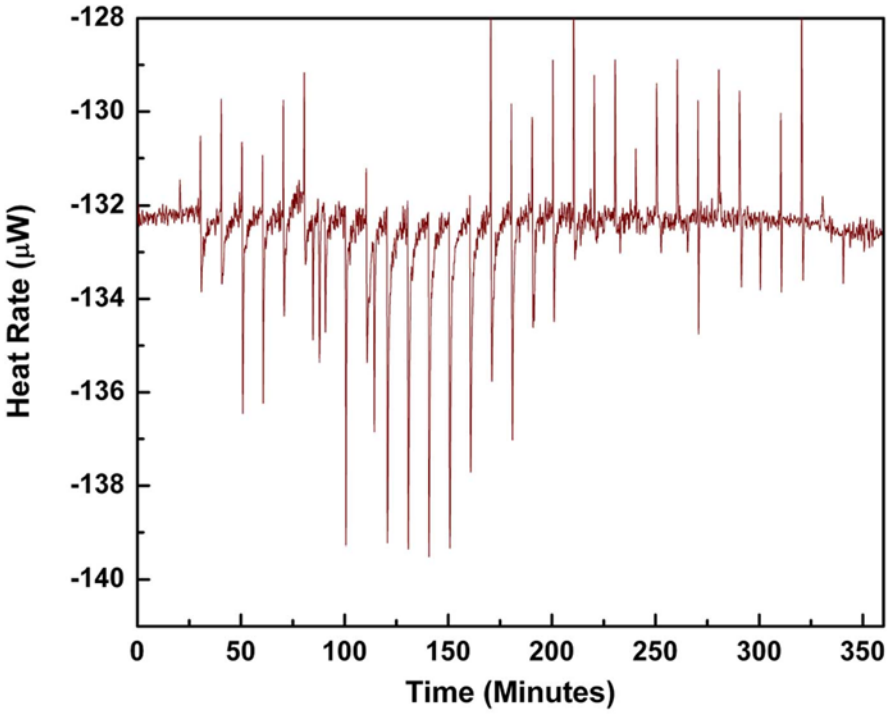

Figure S14 | Calorimetric titration curves of $(Nae\text{-}Npe)_{18}$ into $(Nce\text{-}Npe)_{18}$. The isothermal microcalorimetric experiments were carried out on a Nano ITC (TA Instruments). The sample cell was filled with 1010 μL of 0.2 mM $(Nce\text{-}Npe)_{18}$ solution. 5 μL aliquots of 1.8 mM $(Nae\text{-}Npe)_{18}$ were titrated into the sample cell while the temperature of the system was maintained at 25 °C. The sample cell was stirred at 400 rpm. When the concentration of $(Nae\text{-}Npe)_{18}$ becomes equal to that of $(Nce\text{-}Npe)_{18}$ in the ITC cell, heat was no longer released, indicating that the final composition of the complex is close to 1:1.

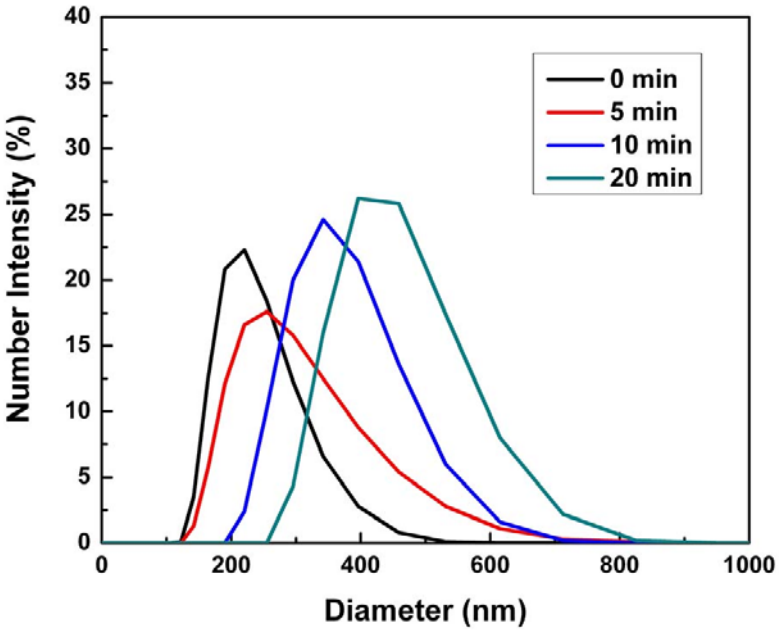

Figure S15 | Size of initial spheres measured by dynamic light scattering. The data was collected from the cloudy solution 0, 5, 10 and 20 minutes after mixing $(Nae\text{-}Npe)_{18}$ and $(Nce\text{-}Npe)_{18}$. Right after mixing (0 minute), the average size of spheres is around 200 nm. The size increases gradually until 20 minutes. One hour after mixing, due to the inhomogeneous size, the size could no longer be measured.

DOI: 10.1038/NMAT2742

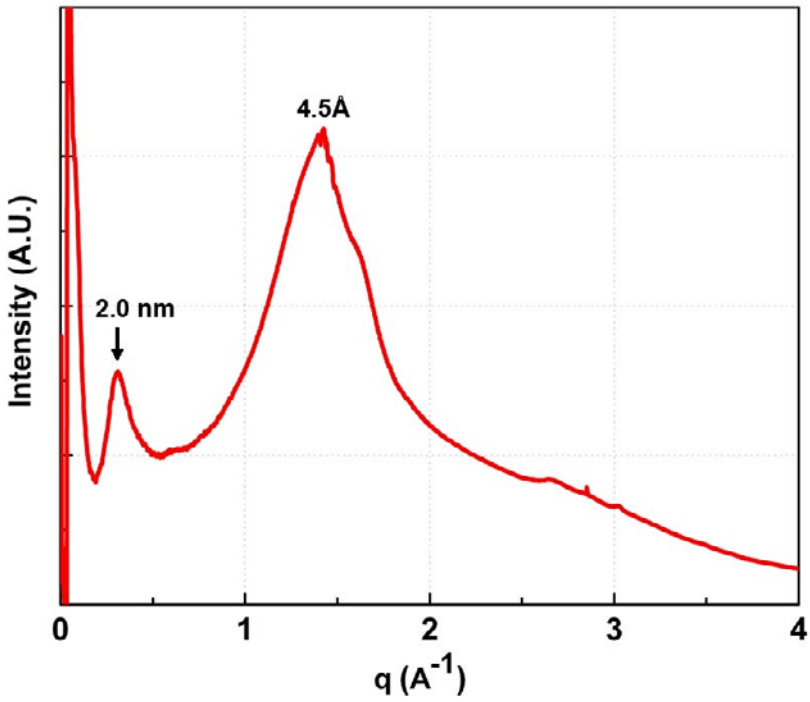

Figure S16 | XRD data of sphere-like complexes formed at early stage of sheet formation. Sphere-like complexes are present in $(Nce\text{-}Npe)_{18}/(Nae\text{-}Npe)_{18}$ solutions immediately after mixing. In order to understand the kinetics of the transformation from aggregate to sheet, the structure of initial aggregates was analyzed. Ten minutes post-mixing x-ray diffraction powder patterns revealed that the initial $(Nce\text{-}Npe)_{18}$ and $(Nae\text{-}Npe)_{18}$ complexes have local ordering with spacings of 2.0 nm and 4.5 Å. The second or third harmonic peaks of 2.0 nm are not observed, while the sheet samples exhibit strong lamellar scattering from 2.7 nm thickness as shown in Fig 4A. This suggests that 2.0 nm ordering in the initial aggregates is not from planar structures.

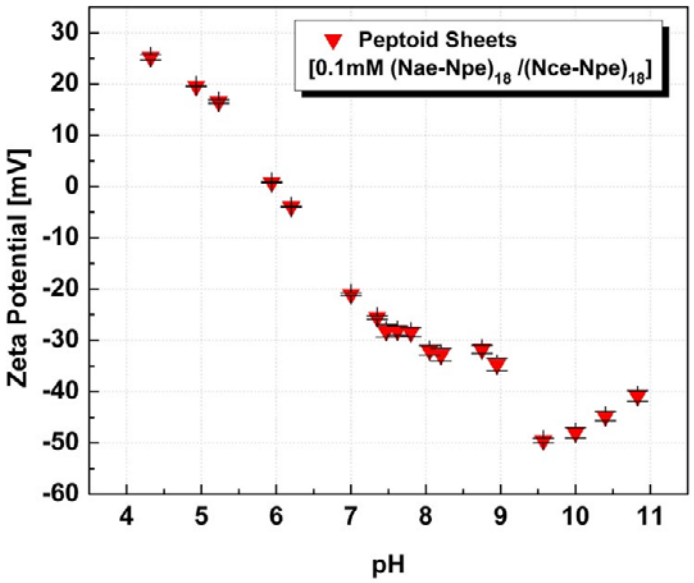

Figure S17 | Zeta potential-pH dependence of peptoid sheets. This analysis revealed an isoelectric point at around pH 6. At the acidic pH of 4.3 zeta potential was relatively large at 25.2 ±0.5 mV, and at the basic pH of 10.83 the zeta potential had a negative value of -40.8±1.1mV.

DOI: 10.1038/NMAT2742

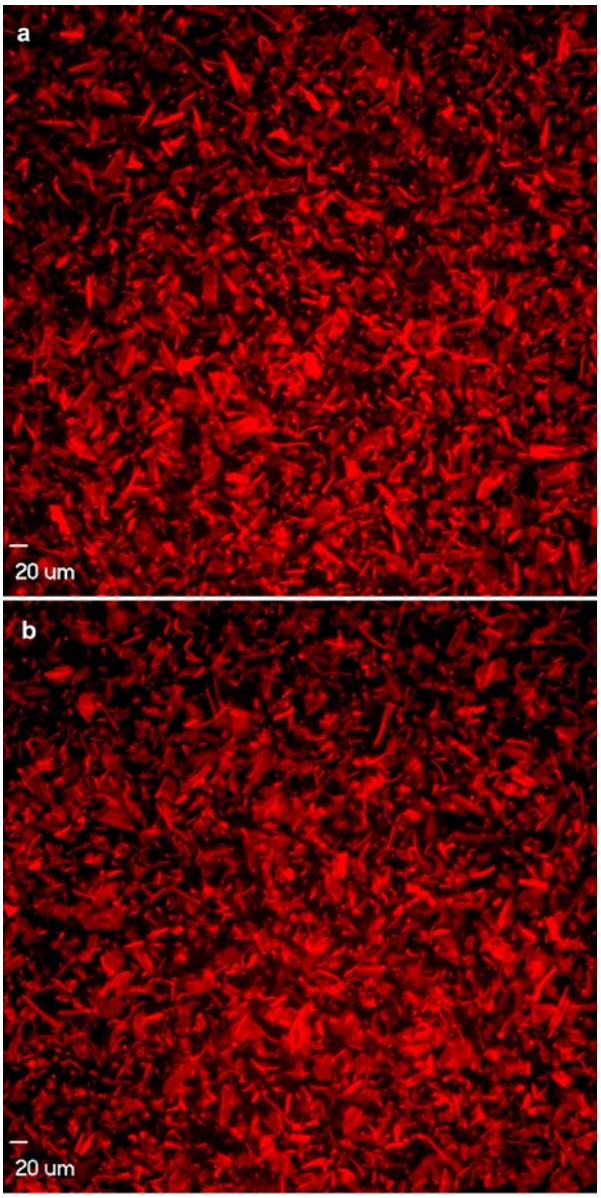

Figure S18 | Fluorescence optical microscope images of sheets that are free floating in aqueous solution. The images **a** and **b** are taken from different areas of the same sample and are representative examples of the number of sheets which can be produced using 0.1mM concentrations of $(Nce\text{-}Npe)_{18}$ and $(Nae\text{-}Npe)_{18}$. The sample was imaged in a small chamber using Nile Red (0.5 μM) as a fluorescent stain and was not further concentrated. Sheet coverage of the microscope slide surface is uniformly high, sometimes forming multiple layers, throughout the sample.